Superalloys 2012: 12th International Symposium on Superalloys
Edited by: Eric S. Huron, Roger C. Reed, Mark C. Hardy, Michael J. Mills, Rick E. Montero, Pedro D. Portella, Jack Telesman
TMS (The Minerals, Metals & Materials Society), 2012

PREDICTION OF INITIAL OXIDATION BEHAVIOR OF NI-BASE SINGLE CRYSTAL SUPERALLOYS: A NEW OXIDATION MAP AND REGRESSION ANALYSIS

A. S. Suzuki[1)*], K. Kawagishi[2)], T. Yokokawa[1)], T. Kobayashi[1)] and H. Harada[1)]
1) Environment and Energy Materials Division, National Institute for Materials Science
1-2-1 Sengen, Tsukuba Science City, Ibaraki, 305-0047, Japan
2) High-Performance Alloys Group, Environment and Energy Material Division/High Temperature Materials Unit,
National Institute for Materials Science 1-2-1 Sengen, Tsukuba Science City, Ibaraki, 305-0047, Japan
*Current Affiliation: Department of Materials, Loughborough University, Loughborough, Leicestershire, LE11 3TU, UK

Keywords: Ni-base superalloy, Oxidation, Chemical potential

Abstract

Predictions for oxidation behavior of Ni-base superalloys are becoming increasingly difficult because of the complex alloy composition. In this study, we focus on the initial oxidation behavior of Ni-base superalloys, and suggest a new oxidation map with using Al and Cr chemical potentials to distinguish the initial oxide type of Ni-base superalloys with seventy binary, ternary, and multicomponent Ni-base single crystal superalloys at 1100 °C. As a comparison of observed and calculated weight changes after one cycle at 1100 °C obtained by a regression analysis, seventy alloys demonstrated two distinct behaviors, which are divided heretofore into group A and group B. Microstructural observation revealed that an oxide layer in the group A alloys consists of Al_2O_3 and/or spinel or complex oxide, whereas an oxide layer in the group B alloys consists of a thick NiO layer with an Al_2O_3 internal subscale. Thermodynamic properties can reflect more effects of alloy elements in Ni-base superalloys, and Al and Cr activities, calculated by Thermo-Calc, were used as factors to distinguish the type of initial oxides. Group A and B alloys can clearly be divided according to Al and Cr activities. This was suggested as a new oxidation map to distinguish the initial oxide type of Ni-base superalloys, and possibly it can apply for any generation of Ni-base superalloys. In addition, empirical equations obtained from regression analysis were suggested to be used for predicting the weight change of alloys after one cycle at 1100 °C, and these could also be applied to all generations of Ni-base superalloys. One equation exhibited excellent agreement between observed and calculated weight changes. The alloys that were applicable for this equation therefore had a compositional dependence.

Introduction

One potential avenue toward higher efficiency gas turbines and jet engines is to increase thermal efficiency of gas turbines and jet engines by increasing the operating temperature. Therefore, oxidation resistance of Ni-base superalloys, which are used as turbine blade and vane applications, is more crucial than before. Recent Ni-base superalloys incorporate refractory elements, and these superalloys can consist of more than 10 elements. The addition of refractory elements to Ni-base superalloys is imperative for maintaining excellent creep properties and microstructural stability at elevated temperature; however, the oxidation behavior of these latest Ni-base superalloys is more complex than was found in previous alloys [1-3] due to these additional elements.

Many models have been suggested to predict the oxidation resistance of Ni-base superalloys for both cyclic and isothermal oxidation [4-6]. However, many of these approaches require specific test conditions, so that practical applications of these approaches are relatively limited. Application to multiple generations of Ni-base superalloys also appears to be particularly controversial.

Giggins, Pettit, and other researchers [7-10] suggested composition effects on the oxidation behavior of Ni-Al-Cr ternary alloys, and this diagram represents oxide types of the ternary alloys depending on the alloy composition. This diagram is useful for predicting the nature of oxides in the case of Ni-base superalloys, however, this is based on only Ni, Al, and Cr composition, as well as a limited application for recent Ni-base superalloys, which contain more elements.

Under cyclic oxidation, the spallation and/or vaporization of oxides are frequently observed, and are strongly associated with these behaviors and oxidation resistance of Ni-base superalloys. The growth rate and adhesion of oxides are greatly different depending on their nature of oxides. It is therefore necessary to incorporate the nature of oxides to establish a more precise and practical life prediction model for oxidation resistance of Ni-base superalloys. The nature of oxides can be distinguished after the first few cycles of cyclic oxidation testing, and the initial oxidation behavior of Ni-base superalloys dominates the overall oxidation behavior of these superalloys.

In this study, we focus on two points concerning the initial oxidation behavior of Ni-base single crystal superalloys: establishing empirical equations for predicting the initial oxidation behavior based on weight change measurements, and suggesting an approach to determine the nature of initial oxides by means of thermodynamic properties [11,12]. Specifically, cyclic oxidation test results of 70 binary, ternary, and multicomponent Ni-base superalloys were used to draw the new oxidation map to distinguish the type of oxides in Ni-base single crystal superalloys. The prediction of oxidation behavior of Ni-base superalloys would benefit greatly from an empirical equation that could define their oxidation resistance, and the map could also serve as a guideline for the development of new alloys that have superior oxidation resistance, as well as allowing more precision in the life prediction of Ni-base superalloys.

Table I: Alloy compositions of selected example alloys (at%).

Alloy	Co	Cr	Mo	W	Al	Ti	Ta	Hf	Re	Ru	C	Ni
EPM-102	13.39	6.07	--	1.89	13.36	0.66	2.8	0.05	2.03	1.88	0.26	Bal.
Ni-30Cr-6Al	--	30.53	--	--	11.77	--	--	--	--	--	--	Bal.
TMS-0	--	--	--	--	18.91	--	--	--	--	--	--	Bal.
TMS-196	6.03	5.61	1.59	1.73	13.17	--	1.96	0.04	2.18	3.14	--	Bal.
TMS-198	6.16	5.78	1.57	1.77	13.46	--	1.94	0.04	1.88	2.23	--	Bal.
TMS-199	6.12	7.66	1.43	1.56	13.15	--	1.93	0.03	1.87	2.22	--	Bal.

Experimental

Seventy Ni-Al binary, Ni-Al-Cr ternary, and multicomponent Ni-base single crystal superalloys from first to fifth generations were used in this study. The alloys were designed and developed via an alloy design program [13] at the National Institute for Materials Science (NIMS) in Japan, and have the following composition ranges: 0-16.9 Co, 0-30.5 Cr, 0-1.9 Mo, 0-4.4 W, 11.5-18.9 Al, 0-2.5 Ti, 0-1.3 Nb, 0-3.6 Ta, 0-0.7 Hf, 0-2.6 Re, 0-5.1 Ru, 0-4.1Si, 0-0.3 C, 0-0.1 B in at%, and the balance Ni. Compositions of selected example alloys [2,14,15] were given in Table I. The alloys were cast into single crystal rods by means of a directional solidification casting furnace, and heat treated with standard two-step treatments.

For the oxidation test, the alloys were cut into cylindrical shapes that were 5 mm in height and 9 mm in diameter. Their surfaces were polished up to #800 SiC paper. Cyclic oxidation testing was conducted at 1100 °C for 1 hour in air and cooled to room temperature for 1 hour in one cycle. The test lasted 200 cycles. The weight of the specimens was measured after each cycle.

The empirical equation suggested in this study was verified using three commercial Ni-base superalloys, which were not included among the 70 tested alloys: CMSX-4, PWA 1480 and TMS-6 [16-18]. These commercial alloys also underwent the same oxidation test as the samples in the present study.

Cross-sectional microstructures and scales formed on the specimen surfaces were observed by scanning electron microscopy (SEM) with a back-scattered electron (BSE) detector.

Thermodynamic properties of the alloys in this study were calculated by Thermo-Calc [19], and the Thermotech Ni-based superalloys database, NI-DATA7 was used for calculation.

Results

Relationships between observed, calculated weight gains and their microstructures

First, regression analysis was performed for all alloys with all alloy elements in at%. A weight change after one cycle at 1100 °C, using Eq. (1) to predict w_1, which is the calculated weight change of alloys after one cycle oxidation test, with 63 % of multiple correlation coefficients was obtained as follows:

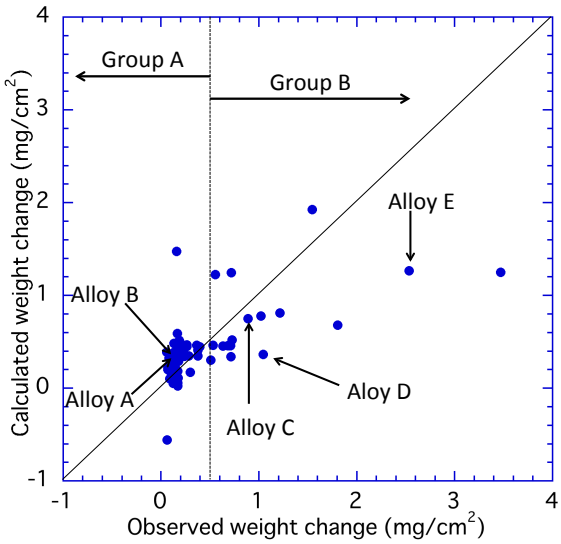

Figure 1: Comparison of observed and calculated weight changes after one cycle. Alloy A through E correspond with the microstructures in Figure 2.

$$w_1 = \Sigma \alpha_i x_i \qquad (1)$$

Where α is the obtained coefficient of each component i from regression analysis, shown in Table II, and x_i is the alloy composition (at%). Table II also shows the values of probability of error, which were determined using α t-test.

The components >10% on the t-test, signifying a larger error, were indicated with '—.' Figure 1 shows a comparison of observed and calculated weight changes after one cycle at 1100 °C. For all the alloy compositions, the empirical equation cannot correctly predict the weight change after one cycle. However, some interesting features were observed. Calculated and observed weight changes of 70 alloys almost can be divided into the following groups depending on their observed weight changes after one cycle, as in Figure 1:

(a) The first group, group A, consists of alloys with the observed weight change with less than approximately 0.5 mg/cm^2.

(b) The second group, group B, consists of the other alloys with the observed weight change with more than 0.5 mg/cm^2.

Table II: The α_i coefficient and t-test values (%) obtained by a regression analysis for all alloys.

	Co*	Cr***	Mo*	W*	Al*	Ti*	Nb*	Ta*	Hf*	Re**	Ru*	Si*	C***
α_i	-6.2x10^{-3}	-0.058	-0.014	0.026	0.1	-0.019	0.13	-0.15	-0.16	-0.22	0.044	-0.15	4.26
t-test	--	0.1	--	--	--	--	--	--	--	1	--	--	0.1

t-test: ***0.1%, **1%, *10%.

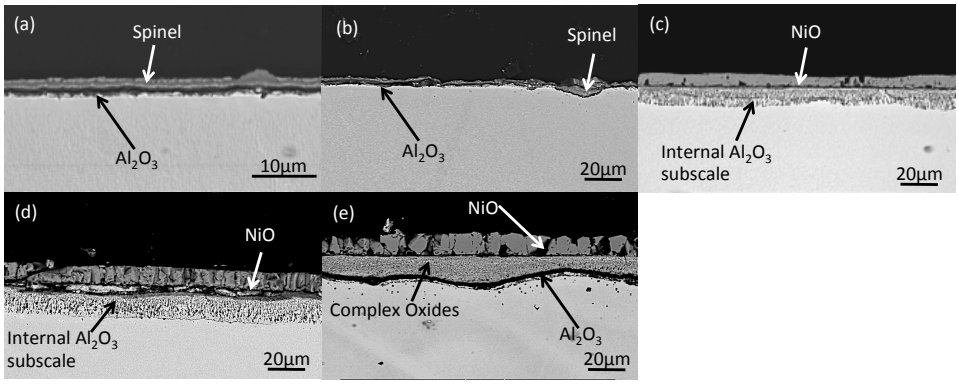

Figure 2: Representative cross-sectional microstructures of (a) Alloy A, (b) Alloy B, (c) Alloy C, (d) Alloy D, and (e) Alloy E after a one cycle oxidation test at 1100 °C.

Also, a calculated weight change of the most alloys in group A after one cycle showed a relatively small deviation from the observed weight change. On the contrary, a calculated weight change of the alloys in group B after one cycle showed a large deviation from the observed weight change, and the deviation tend to be large, as the alloys in group B have the larger observed weight change after one cycle. Group classifications of the selected example alloys in Table I include the following: Ni-30Cr-6Al, TMS-196, TMS-198, and TMS-199 for group A, and EPM-102 and TMS-0 for group B.

Figure 2 shows representative cross-sectional oxide morphologies of alloys in groups A and B after one cycle of oxidation testing (Their prediction behavior was mentioned in Figure 1.). Note that alloy A, C, and E are fourth generation alloys whereas alloy B and D are fifth generation alloys. Alloy A and B in Figure 2 (a) and (b) were randomly chosen from Group A. From Group B, alloy C was selected due to the relatively small deviation between calculated and observed weight changes, whilst alloys D and E were due to the large deviation in Figure 1. With regard to alloys A and B, both alloys demonstrated relatively small deviation between the observed and calculated weight changes, and are located within the group of data where most of the group A alloys are.

Alloys showed similar phase constitutions of oxide layers, respectively, in each group after one cycle in Figure 2. However, it should be noted that constitutions of the oxide layers between groups A and B alloys were significantly different. Alloys in group A in Figures 2(a) and (b) developed a thin Al_2O_3 layer and/or spinel or complex oxides on the specimen surface. Similar oxides are observed in TMS-196 [14] and TMS-198 [3], and for TMS-196, Ni(Al,Cr)O as a spinel oxide was observed with continuous Al_2O_3 formation. On the contrary, the alloys in group B in Figures 2(c) through (e) formed a thick NiO oxide layer at the top of the surface with approximately 10 μm thickness, followed by either Al_2O_3 or a complex oxide internal subscale. Specifically, alloy E in Figure 2(e) consists of mostly discrete particles under the thick NiO layer, and a thin Al_2O_3 layer at the interface between the substrate and the internal subscale oxide layer. The internal subscale oxide layer formed when oxygen from the atmosphere diffused through the NiO scale. The similar morphology was reported by Pruessner in a third generation Ni-base single crystal superalloy, TMS-75 [20]. These oxide morphologies observed in Figure 2 are comparable with other Ni-base superalloys, and more characterizations of the oxides were reported [14,20,21]. Some alloys in group A, e.g. Alloy B in Figure 2(b), also partially formed a NiO layer; however, the thickness and area fraction of the NiO layer is far less than the alloys in group B. In fact, group B alloys showed more than 0.5 mg/cm^2 of an observed weight change after one cycle oxidation test. The large weight gain after one cycle in group B alloys would be derived from the formation of the thick NiO layer, and this behavior is consistent with microstructural observations in Figure 2.

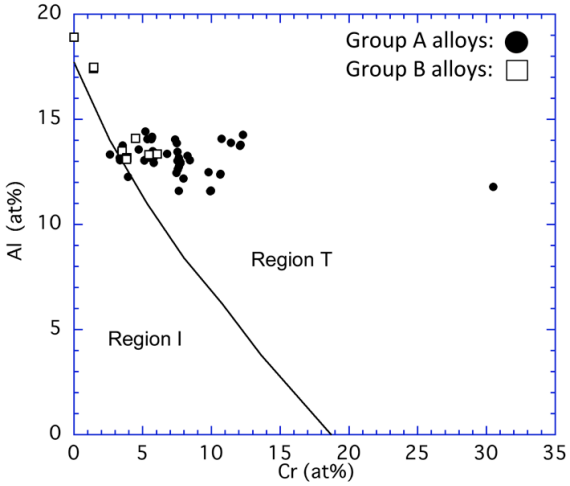

Figure 3: Al and Cr compositions of alloys used in this study. The solid line represents the border lines suggested by Giggins et al..

A new oxidation map for initial oxidation of Ni-base superalloys

Figure 3 shows a diagram plotting compositions of Al and Cr (at%) in the alloys used in this study. The solid line within Figure 3 represents the borderline of region I, consisting of mostly NiO, and region T, NiO, $NiCr_2O_4$, $NiAl_2O_4$, and Al_2O_3 transition in the diagrams suggested by Giggins et al. and other researchers [7-10]. As Figure 3 shows, most of the alloys in both groups A and B are located in region T, and should consist of Al_2O_3 and spinel in the oxide layer. Some group B alloys

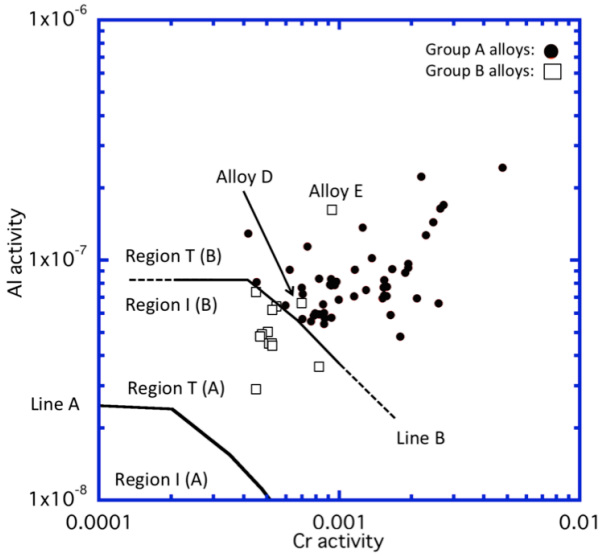

Figure 4: Relationship between Al activity and Cr activity of 70 Ni-base superalloys. Line A represents the border determined by Ni-Al-Cr ternary diagrams whereas Line B represents the border between Region I and Region T determined in this study.

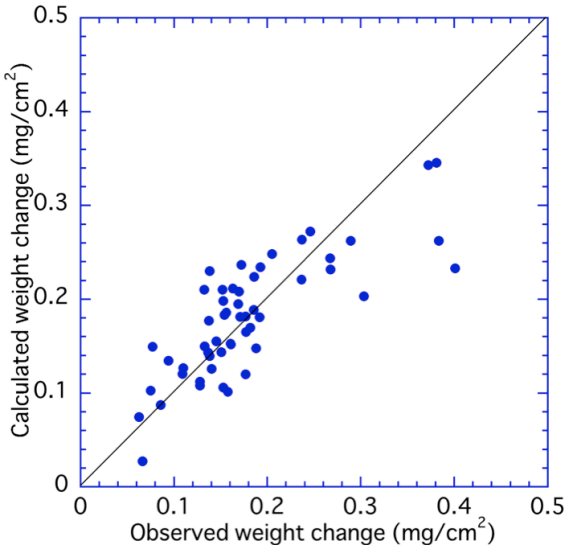

Figure 5: Comparison of observed and calculated weight changes for group A alloys.

tend to align near region I; however, many of the group A and B alloys overlapped each other. This indicates that the type of initial oxide formed in Ni-base superalloys cannot precisely be explained with only Al, Ni, and Cr compositions.

Thermodynamic properties strongly influence the initial oxidation behavior of Ni-base superalloys, and reflect a greater effect of alloy elements, added to Ni-base superalloys. It is fascinating to see how the thermodynamic properties relate to each other with respect to the initial oxide formation of Ni-base superalloys. Al and Cr were selected as thermodynamic properties because these properties can be important factors to influence Al_2O_3 and Cr_2O_3 formations, which are working as a protective oxide scale in Ni-base superalloys. In addition, high Cr-containing Ni-base superalloys potentially form Cr_2O_3 on the specimen surface after oxidation, and the diagram [8] also includes region II, consisting of Cr_2O_3. Relationships between Al and Cr activities were investigated as in Figure 4. In Figure 4, line A represents the border calculated from Ni-Al-Cr ternary diagrams [8] for the separation of region I and T, whereas line B indicates the border of region I and T as suggested in this study. In fact, line A aligned at a lower position than line B in Figure 4, and alloys in group A and B can be classified the type of initial oxide more clearly with line B. This suggests that the initial oxide type in Ni-base superalloys can be determined via line B, and line B reflects additional compositional effects added to Ni-base superalloys more than is accounted for by line A.

'Alloy D' and 'Alloy E' of group B alloys were outliers with regard to this classification scheme; however, this might be because of the high amount of Co for Alloy E and the high amounts of Re and Ru for Alloy D, respectively. Additional modification and investigation for this diagram will be conducted in the future; however, this diagram can be a representative to indicate the type of initial oxides for Ni-base superalloys, which can be applicable for any generation of Ni-base superalloys.

Regression analysis for Group A and B

For group A, all alloy compositions in at%, except for Ni and Hf, were used for regression analysis to obtain Eq. (1) with the coefficients listed in Table III. Figure 5 shows a comparison of the observed and calculated weight changes of the alloys. In general, Hf is effective at improving oxidation resistance of Ni-base superalloys [1,22]. However, Hf was excluded from the components or regression analysis in the present study since it did not show a strong effect for regression analysis. Most of the alloys used in this study contain less than 0.05 at% of Hf, meaning that very little variation occurred in the range of Hf content compared to the other components in the Ni-base superalloys used here. Using low diversity of values in regression analysis results in low reliability and a low regression coefficient.

Table IV: Comparison of observed and calculated weight changes of commercial Ni-base superalloys, obtained from Eq. (1) and the α_i coefficients in Table III.

Alloy	Observed weight change (mg/cm^2)	Calculated weight change (mg/cm^2)	Error (%)
TMS-6	0.109	0.11	1.38
CMSX-4	0.186	0.183	-1.8
PWA1484	0.211	0.228	7.95

Table III: α_i coefficient and t-test values (%) obtained by a regression analysis for group A alloys.

	Co*	Cr***	Mo***	W***	Al***	Ti**	Nb***	Ta*	Re***	Ru*	Si*
α_i	$4.6x10^{-3}$	0.013	0.13	0.088	-0.032	0.056	0.11	0.027	0.075	$-9.5x10^{-4}$	-0.025
t-test	--	0.1	0.1	0.1	0.1	1	0.1	--	0.1	--	--

Table V: Comparison of observed and calculated weight changes for group B alloys.

	Co*	Cr*	Mo*	W*	Al*	Ta*	Re*	Ru*
α_i	-0.015	0.31	-1.01	1.36	0.078	-0.52	-0.96	0.25
t-test	--	--	--	--	--	--	--	--

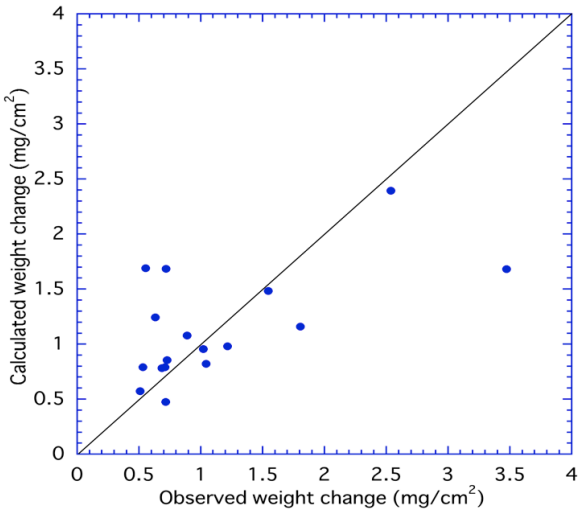

Figure 6: Comparison of observed and calculated weight changes for group B alloys.

Therefore, the Hf content was not suitable for regression analysis in the present study. Regression analysis for group A showed a multiple correlation coefficient of 80%, and Figure 5 also shows good correspondence between the observed and calculated weight changes. Most t-test values listed in Table III also indicate the smallest probability of error, at 0.1%. Some alloy elements, such as Co, Ru and Si, showed a larger value for the t-test (Table III). In general, larger t-test values were obtained when alloys had a less diverse composition and fewer alloys contained the elements, such as Si.

Some of the α_i coefficients shown in Table III agree well with the general oxidation behavior of alloy components in Ni-base superalloys: superior oxidation resistance of Ni-base superalloys can be achieved by a uniform and continuous thin formation of Al_2O_3, resulting in a smaller weight change during oxidation. In Table III, a negative value of α_{Al} (α_{Al}=-0.03) minimizes the weight gain due to oxide formation, and this corresponds well with the general oxidation behavior of Ni-base superalloys. As other examples, Mo (α_{Mo} = 0.13) and Nb (α_{Nb} = 0.11), which generally tend to degrade the oxidation resistance of Ni-base superalloys, exhibited relatively larger coefficients of α_i than did the other components in Table III, and these elements would be expected to contribute to a larger mass gain upon oxidation.Thus, the behavior of group A alloys has a high dependence on the alloy composition.

For group A alloys, Eq. (1) and α_i coefficients in Table III were validated with three commercial Ni-base superalloys: TMS-6, CMSX-4 and PWA 1484. These were tested under the same experimental conditions as the 70 test alloys. Their observed and calculated weight changes, which were obtained with Eq. (1) and the α_i coefficients in Table III, are given in Table IV. TMS-6 and CMSX-4 specifically demonstrated the smallest error between the observed and calculated weight error of less than 2%. Thus, the three commercial Ni-base superalloys exhibited an excellent correspondence between the observed and calculated weight changes. Therefore, the empirical equation appears to be beneficial for predicting the initial oxidation behavior of group A Ni-base superalloys.

Fewer alloys were found in group B than in group A, and a reduction of components was required to perform regression analysis. We chose Co, Cr, Mo, Al, W, Ta, Re and Ru for the analysis, as these are considered as basic components of Ni-base superalloys. The regression analysis yielded an empirical equation for group B alloys with a multiple correlation coefficient of 61%. Figure 6 shows a comparison of observed and calculated weight changes for group B alloys after one cycle, and Table V shows the coefficients for α_i and t-test values for each component obtained from the regression analysis. Comparing each coefficient, relatively large coefficients of α_i were found for Re, W and Mo compared to the other alloy elements, which suggested that these contributed to the increase in weight change after one cycle, and this corresponds with the observed results. However due to the lower reliability of t-test values in Table V, more alloys should be added to enhance the reliability of the equation and α_i coefficient. Testing of a greater number of alloys from group B is necessary to establish the empirical equations with higher accuracy and this will be carried out in the future.

In the present study, we established two empirical equations that depend on the observed initial weight changes and allow prediction of initial weight changes of alloys after one cycle at 1100 °C. These equations appear to be applicable for all generations of alloys, and have fewer restrictions than the other approaches used to predict weight changes of Ni-base superalloys after oxidation. The equations will be further refined in future research.

Discussion

The oxidation behavior of Ni-base superalloys is generally considered similar to that of a Ni-Cr-Al ternary alloy system, because Ni-base superalloys contain various elements, including Co, Cr, Al, Ti, and W. Recent Ni-base superalloys, particularly after the third generation, contain more solid solution-strengthening elements, such as Re, Mo, and Ru. Nevertheless, some of these elements degrade the oxidation resistance of Ni-base superalloys [2,23]. For example, adding Mo to third generation alloys deteriorates their oxidation resistance because of the formation of Mo oxide, which is more prone to volatilization. In addition, each alloying element, consisting of Ni-base superalloys, has a different partition behavior [24], which would also affect the initial oxidation resistance of Ni-base superalloys. The complexity of the alloy composition of Ni-base superalloys increases the difficulty in estimating the oxidation behavior of current Ni-base superalloys with conventional Ni-Al-Cr ternary diagrams [8].

The initial oxidation behavior of Ni-base superalloys is a crucial factor in determining the longevity of turbine blades, and the

oxidation behavior of Ni-base superalloys can vary depending on the alloys. As in Figures 1 and 2, alloys forming Al_2O_3 and/or spinel oxides showed a relatively small initial observed weight change, whereas alloys forming thick NiO tended to show a large mass gain because of the formation of NiO oxides.

NiO is a non-protective oxide, and is porous in nature. This means that NiO provides greater oxygen access to the underlying metals, resulting in continued oxidation. NiO formation in Ni-base superalloys thus leads to more spallation of oxides after cycles, which causes continuous mass loss and poor oxidation resistance.

On the contrary, Al_2O_3 and/or spinel or complex oxide forming Ni-base superalloys tend to show less spallation than the thick NiO forming alloys because Al_2O_3, formed at the metal–oxide interface, has better adhesion than NiO, and works as a protective oxide.

At least two factors form a continuous and protective scale on an alloy surface. The transition from internal to external oxidation is well described by Wagner and the other researchers [8,25-28], and the velocity of the reaction front of the internal subscale depends on oxygen solubility and initial solute concentration. The first criteria for the transition from internal to external oxidation in a Ni-Al alloy is expressed as follows:

$$N_{Al}^{(1)} \geq \left[\frac{\pi g^*}{3} N_O \frac{D_O V_m}{\widetilde{D}_{Ni-Al} V_{AlO1.5}}\right]^{1/2} \quad (2)$$

where N_O is oxygen solubility in the alloy, D_O is the diffusivity of oxygen in alloy (cm^2s^{-1}), $\widetilde{D}_{Ni-Al}$ is the alloy interdiffusion coefficient, V_m and $V_{AlO1.5}$ are the molar volume fraction of the alloy and oxide. g^* is a critical value; the transition from internal to external oxidation occurs, and is generally 0.3 [8]. Here, the molar volume solvent metal V_m is an important factor, and an alloy must have an enough Al concentration to form continuous Al_2O_3 on the specimen surface. However, Figure 3 revealed that neither Al nor Cr compositions of the 70 alloys explain the differences of oxide morphology, and it can be assumed that the complexity of alloy composition in Ni-base superalloys has other effects on initial oxide morphology. In this study, Al and Cr activities were used to distinguish initial oxide types. For the diffusion of an A-B alloy, an activity of elements is also strongly associated with this, and the relationships between activity and diffusion coefficients can be expressed by the following Darken-Harty-Crank relation [29,30]:

$$\widetilde{D} = (X_B D_A + X_A D_B)$$

where

$$\phi = 1 + \frac{d \ln \gamma_A}{d \ln X_A} = 1 + \frac{d \ln \gamma_B}{d \ln X_B} \quad (3)$$

where γ_A is the thermodynamic activity coefficient of element A, and X_A represents the mole fraction of A. An increase in the activities of certain elements, such as Al, would be expected to promote more diffusion of the elements if the oxidation observed in this study is dominated by the diffusion process of alloy elements. In addition to the molar volume solvent, an activity is a potentially important factor that causes external oxidation.

Second, scale growth should also be considered. A diffusion of certain elements in the alloys has to be fast enough to supply the solute elements to maintain a continuous external scale, whereas the solute element is consumed by the scale growth. Assuming that Al_2O_3 is formed in the alloys, the minimum concentration can be expressed as follows:

$$N_{Al}^{(2)} = \frac{V_m}{32V}\left(\frac{\pi k_p}{\widetilde{D}_{Ni-Al}}\right) \quad (4)$$

where k_p is an oxidation constant of a parabolic low, and is measured scale thickness. If the Al concentration is higher than $N_{Al}^{(2)}$, then Al_2O_3 formation is possible. In this study, 70 alloys are categorized into groups A and B. The range of Al concentration in group A is 11.17 to 14.40 at%, whereas the range in group B is 13.1 to 18.91 at%, which are slightly higher than in group A. Smaller vales of V_m enable lower $N_{Al}^{(2)}$ suggesting that group A alloys can form and maintain protective Al_2O_3 formations on the alloy surface with a lower Al concentration. Likewise, smaller k_p and higher $\widetilde{D}_{Ni-Al}$ in group A alloys than those in group B alloys would enable the formation of Al_2O_3 with less Al in the substrates. Ni-base superalloys consist of more complex alloy compositions; however, these compositions would explain the differences in oxidation mechanisms and why the initial oxide types can be divided with Al and Cr activities.

Developments of Ni-base single crystal superalloys have progressed with changing alloy compositions. A new element will be added to improve their high temperature capabilities; however, the addition of new elements to the alloys occasionally overturns their oxidation behavior. In this study, various first to fifth generation of Ni-based superalloys were used, and both group A and B alloys contain all generations of the alloys. However, it should be noted that group B contains more fourth and fifth generation alloys than the previous generation alloys. This indicates that change of alloy composition in fourth and fifth generation alloys may promote NiO formation as an initial oxide layer, and fourth and fifth generation alloys tend to be categorized to group B, rather than Group A. Fourth and fifth generations of Ni-base superalloys can be characterized to contain more refractory elements, such as Mo, Re and Ru, and less Cr content, comparing alloy compositions between different generations of Ni-base superalloys. Cr is generally considered as an important element to enhance oxidation resistance [32], whereas Re and Mo tends to degrade oxidation resistance of Ni-base superalloys. With regard to Ru, the effects are still controversial [1-3,21], however, some studies [1,21] reported that Ru-containing Ni-base superalloys show inferior oxidation resistance than the previous generation alloys, although Ru provides excellent microstructure stability that allows further addition of alloying elements for higher strength at an elevated temperature [33]. It would be rationalized that less Cr and high Mo, Re and Ru contents in later generation of Ni-base superalloys could effect for initial oxidation of Ni-base superalloys. A prediction or model of the oxidation behavior, based on alloy composition, thus should correspond to such changes.

In this study, the thermodynamic properties of Ni-base superalloys, which were calculated by Thermo-Calc, were used to distinguish the initial oxide type of the alloys, instead of a Ni-Cr-Al ternary diagram based on alloy composition. The method in this study can correspond to additions of new elements and/or changes in alloy composition, as far as the database for the

elements is available. Also, the Al and Cr activities from Thermo-Calc can reflect these changes in alloy elements. High consistency between the predicted and the observed oxide types of 70 binary, ternary, and multicomponent Ni-base superalloys would be a good example, showing that the Al and Cr activities from Thermo-Calc contain various changes in the alloy elements.

In addition, the empirical equations indicated the effect of the alloy composition of group A and B alloys, respectively, on the initial mass gain via regression analysis, and some elements, such as Al, Nb, and Mo, demonstrated a good agreement between the general oxidation behavior of Ni-base superalloys and the prediction for group A alloys. Because of a lack of the number of group B alloys, it is not possible to clarify whether or not group B alloys have compositional dependence on the initial oxidation behavior. Nevertheless, the following exceptions were noted between the predictions in this study and their microstructures: Alloy D and Alloy E as shown in Figure 4. Alloy E in Figure 2(e) contains a relatively high amount of Co, and Alloy D in Figure 2(d) contains the second highest amount of Co, compared with the other alloys in group B. Co is known as an element that degrades the oxidation resistance of Ni-base superalloys, because CoO grows faster than NiO [34]. Kawagishi also reported that a high amount of Re in substrate degrades the oxidation resistance of Ni-base superalloys [2]. High amounts of Re and Ru are generally present in the group B alloy. An extreme amount of Co, Ru, and Re and the combination of certain elements in Alloys D and E might be associated with the deviations in Figure 4. Al and Cr activities in this study were determined with all alloy compositions via Thermo-Calc. A single element, a combination of certain elements, and the balance between them would reasonably affect the activities. Future study is planned to investigate how each element and/or some combinations of elements relate to these activities, which would elucidate the reason for the deviation between the activities and the initial oxide formation of Alloys D and E.

Group A and B alloys can clearly be separated in Figure 4, by the border used to separate Region I and Region T, which is suggested by line B (and shown in Figure 4) in this study. Where line B is exactly aligned and how line B for Ni-base superalloys is drawn cannot precisely be determined from Figure 4, and it should be noted that line B is a provisional line to separate Regions I and T for 70 Ni-base superalloys in this study. Line B is aligned in a higher position than line A, which was calculated from the Ni-Al-Cr ternary diagrams suggested by Giggins et al. [8]. Compared with line A, additional elements into Ni-base superalloys increases the Al and Cr activity, and this therefore shifted the position of line B, which is the border between Region T and I in Figure 4. These increases should be reflected in order to develop models and/or life predictions for the oxidation behavior of the latest Ni-base superalloys.

The new oxidation map for Ni-base superalloys in Figure 4, drawn with Al and Cr activities instead of their atomic concentrations, suggested throughout this study would be useful for predicting their initial oxidation resistance. However, it must be noted that this diagram can be applied only for initial oxidation, not for long-term oxidation resistance of Ni-base superalloys. Mass loss in cyclic oxidation test happens as a result of the spallation and/or vaporization of oxides formed on specimen surfaces. Even if some alloys show relatively better oxide morphologies with smaller weight changes in the first few cycles, the oxide constitutions and morphology may change once the spallation of oxides starts. This possibly results in changes in the oxide constitution from Regions T to I, suggesting the change of oxidation mechanism. In addition, once continuous mass loss occurs as a result of the spallation of oxides, it is impossible to predict mass loss behavior with the approach used in this study. The spallation of oxides has a considerably different mechanism, and the driving force for spallation differs from the driving forces for the formation of oxides as mentioned earlier. The map in Figure 4 does not contain information related to the spallation of oxides, and Al and Cr activities calculated in this study are based on nominal composition. The oxidation map suggested in this study to distinguish the oxide types of Ni-base superalloys is therefore only valid for the initial oxidation stage, which is before spallation occurs. However, again, it should be noted that the map suggested in this study can be applicable for any generation of Ni-base superalloys, as Al and Cr activity includes the effects of elements such as Re and Ru. This makes it possible to distinguish the initial oxide type of new alloys without any tests. Thus, it would contribute to further developments of both Ni-base superalloys with superior oxidation resistance and life predictions of the oxidation resistance in the future.

Conclusions

A new oxidation map to distinguish the type of initial oxide formation in Ni-base superalloys and empirical equations were suggested in this study. Seventy Ni-Al binary, Ni-Al-Cr ternary, and multicomponent Ni-base superalloys from first to fifth generations for oxidation tests and calculated thermodynamic properties by Thermo-Calc were used in this study, and the following results and observations were obtained:

1. A new oxidation map to distinguish the initial oxide type of Ni-base superalloys was drawn with Al and Cr activity, instead of their concentrations, and we succeeded in dividing the alloys into two groups depending on the oxide type.

2. Al and Cr activities include the effect of alloy elements, such as Re and Ru, and the diagram suggested in this study can be applicable for any generation of Ni-base superalloys.

3. The observed borderline separating Region I (mostly NiO) and Region T (Al_2O_3, and/or spinel or complex oxides), which is suggested in this study, was found to occur at a higher position relative to both Al and Cr activities than the calculated borderline from the Ni-Al-Cr diagram. It was also observed that when higher alloy element levels were added to these Ni-base superalloys, the borderline was shifted further upwards.

4. An empirical equation for group A was obtained with a multiple correlation coefficient of 80%, and the calculated weight change after one cycle corresponded well with the observed weight changes. The oxidation behavior of group A alloys therefore shows a high dependence on alloy composition.

Acknowledgements

Authors would like to acknowledge Prof. Rachel Thomson in Loughborough University for the wonderful suggestions for this work.

References

1. K. Kawagishi, H. Harada, A. Sato, A. Sato, and T Kobayashi. "The Oxidation Properties of Fourth Generation Single Crystal Ni-Based Superalloys," *JOM,* Jan (2006), 43-46.

2. K. Kawagishi, A. Sato, A. Sato, T. Kobayashi, and H. Harada. "Oxidation Behavior of Ru-Cotaining Ni-Base Single Crystal Superalloys," *Materials Science Forum,* 522-523 (8) (2006), 317-322.

3. K. Kawagishi, A. Sato, H. Harada, A.C. Yeh, Y. Koizumi, and T. Kobayashi. "Oxidation Resistant Ru Containing Ni-Base Single Crystal Superalloys," *Materials Science Technology*, 25 (2) (2009), 271-275.

4. B.A. Pint, P.F. Tortorelli, and I.G. Wright. "Effect of Cycle Frequency on High-Temperature Oxidtion Behavior of Alumina-Forming Alloy," *Oxidation of Metals,* 58 (1/2) (2002), 73-101.

5. C. Wagner, "Theoretical Analysis of the Diffusion Processes Determining the Oxidation Rate of Alloys," *Journal of Electrochemical Society,* Oct (1952), 369-380.

6. J.L. Smialek, J.A. Nesbitt, C.A. Barrett, C.E. Lowell. "Cyclic Oxidation Testing and Modelling: A NASA Lewis Perspective." *NASA report*, No. 209768 (2000).

7. C.S. Giggins, and F.S. Pettit. "Oxidation of Ni-Cr-Al Alloys Between 1000 and 1200 °C," *Journal of Electrochemical Society,* 118 (11) (1971), 1782-1790.

8. C.T. Sims, N.S. Stoloff, and W.C. Hagel. *Superalloys II.* (A Willy-Interscience Publication, New York, 1987), 293-326.

9. G.R. Wallwork, and A.Z. Hed. "Some Limiting Factors in the Use of Alloys at High Temperature," *Oxidation of Metals*, 3(2) (1971), 171-184.

10. C.A. Barrett, and C.E. Lowell. "Resistance of Ni-Cr-Al Alloys to Cyclic Oxidation at 1100 and 1200°C," *Oxidation of Metals,* 11 (4) (1977), 199-223.

11. A.S. Suzuki, K. Kawagishi, T. Yokokawa, H. Harada and T. Kobayashi. "Prediction of initial oxidation behavior of Ni-base single crystal superalloys by regression analysis," *Scripta Materialia*, 65 (2011), 49–52.

12. A.S. Suzuki, K. Kawagishi, T. Yokokawa, T. Kobayashi and H. Harada. "A New Oxide Morphology Map: Initial Oxidation Behavior of Ni-Base Single-Crystal Superalloys", *Metallurgical and Materials Transactions A*, 43, (1) (2012), 155-162.

13. H. Harada, K. Ohno, T. Yamagata, T. Yokokawa, and M. Yamazaki. "Phase Calculation and its Use in Alloy Design Program for Nickel-Base Superalloys," *Superalloys 1988* (Warrendale, Champion, PA, TMS, 1988), 733–744.

14. A. Sato, H. Harada, A.C. Yeh, K. Kawagishi, T. Kobayashi, Y. Koizumi, T. Yokokawa, and J.X. Zhang. "A 5th generation SC Superalloys with Balanced High Temperature Properties and Proccessability," *Superalloys 2008*, (Warrendale, Champion, PA, TMS, 2008), 131–138.

15. S. Walston, A. Cetal, R. Mackay, K. O'Hara, D. Duhl, and R. Dreshfield. "Joint Development of a Fourth Generation Single Crystal Superalloy," *Superalloys 2004* (Warrendale, Champion, PA, TMS, 2004), 15–24.

16. K. Harris, R.E. Schwer, and G.L. Erickson. "CMSX Single Crystal, CM DS & Integral Wheel Alloys Properties and Performance," *High Temperature alloys for Gas Turbines and Other Applications*, (Springer, proceedings of a conference held in Liège, Belgium, 6-9 October 1986, vol. 1), 709-728.

17. A.D. Cetel, D.N. Duhl. "SECOND-GENERATIONNICKEL-BASE SINGLE CRYSTAL SUPERALLOY," *Superalloys 1988*, (Warrendale, Champion, PA, TMS, 1988) 235-244.

18. T. Yamagata, H. Harada, S. Nakazawa, M. Yamazaki. "Alloy Design for High Strength Nickel-base Single Crystal Alloys," *Superalloys 1984*, (Warrendale, Champion, PA, TMS, 1984), 157-166.

19. *Thermo-Calc Software*: Thermo-Calc, http://www.thermocalc.se/.

20. K. Pruessner, and H. Harada. "Microstructural Observations on Oxidized Ni-Based Superalloy TMS-75 and Pgm-Doped Derivatives," *Journal of Electrochemical Society,* 57 (11) (2010), 95-98.

21. K. Kawagishi, A. Sato, T. Kobayashi and H. Harada. "Oxidation Properties for 2-5th Generation Ni-Base Single Crystal Superalloys at 1023, 1073, 1373K," *Journal of Japan Institution of Metals,* 71 (3) (2007), 313-319.

22. J. R. Nicholls. "Designing Oxidation-Resistant Coatings." *JOM*, January (2000), 28-35.

23. R. Hashizume, A. Yoshinari, T. Kiyono, Y. Murata, and M. Morinaga. "Development of Ni-Based Single Crystal Superalloys for Power-Generation Gas Turbines," *Superalloys 2004*, (Warrendale, Champion, PA, TMS, 2004), 53-62.

24. T. Yokokawa, M. Osawa, K. Nishida, T. Kobayashi, Y. Koizumi, and H. Harada. "Partitioning Behavior of Platinum Group Metals on the γ and γ' Phase of Ni-Base Superalloys at High Temeperature," *Scripta Materialia,* 49 (2003), 1041-1046.

25. F.H. Stott, G.C. Wood, D.P. Whittle, B.D. Bastow, Y. Shida, and A. Martinez-Villafane. "The Transport of Oxygen to the Advancing Internal Oxide Front During Internal Oxidation of Nickel-Base Alloys at High Temperature," *Solid State Ionics,* 12 (1984), 365-374.

26. F.H. Stott Y. Shida, D.P. Whittel, G.C. Wood, and B.D. Bastow. "The Morphological and Structural Development of Internal Oxides in Nickel-Aluminium Alloys at High Temperatures," *Oxiation of Metals,* 18 (3/4) (1982), 127-146.

27. F. H. Stott, G.C. Wood, Y. Shida, D.P. Whittle, and B.D. Bastow. "The Depelopment of Internal and Intergranular Oxides in Nickel-Chromium-Aluminium Alloys at High Temperature," *Corrosion Science,* 21 (8) (1981), 599-624.

28. N. Birks, and G. H. Meier. *Introduction to High Temperature Oxidation of Metals.* 2nd edition ed. (London: Edward Arnold, 1983), 91-130.

29. L.S. Darken. "Diffusion, mobility and their interrelation through free energy in binary metallic systems," *Transactions of AIME*, 175 (1948), 184–201.

30. G.S. Hartley and J. Crank. "Some fundamental definitions and concepts in diffusion processes," *Transactions of Faraday Society*, 45 (9)(1949), 801–818.

31. K. Kawagishi, A. Sato, T. Kobayashi and H. Harada. "Temperature Dependence of Oxidation Properties for 5th Generation Ni-Base Single-Crystal Superalloys," *Journal of Japan Institution of Metals*, 70 (8) (2006), 686–689.

32. F.H. Stott, G.C. Wood, J. Stringer. "The Influence of Alloying Elements on the Development and Maintenance of Protective Scales," *Oxidation of Metals,* 44(1/2) (1995), 113-145.

33. Y. Koizumi, T. Kobayashi, T. Yokokawa, J. Zhang, M. Osawa, H. Harada, Y. Aoki, and M. Arai. "DEVELOPMENT OF NEXT-GENERATION NI-BASE SINGLE CRYSTAL SUPERALLOYS," *Superalloys 2004*, (Warrendale, Champion, PA, TMS, 2004), 35-43.

34. S. Bose. *High Temperature Coatings,* (Burlington, USA: Butterworth-Heinemann. Burlington, MA, 2007), 29–52.